

# Tree taxa and pyrolysis temperature interact to control the efficacy of pyrogenic organic matter formation

Pierre-Joseph Hatton · Subhasish Chatterjee · Timothy R. Filley · Keyvan Dastmalchi · Alain F. Plante · Samuel Abiven · Xiaodong Gao · Caroline A. Masiello · Steven W. Leavitt · Knute J. Nadelhoffer · Ruth E. Stark · Jeffrey A. Bird

Received: 30 March 2016/Accepted: 12 September 2016/Published online: 23 September 2016 © Springer International Publishing Switzerland 2016

**Abstract** We know little about how shifts in tree species distribution and increases in forest fire intensity could affect the formation of pyrogenic organic matter (PyOM) or charcoal, one of the most important and persistent soil organic matter pools. This limitation arises partly because the role of the precursor wood in controlling PyOM formation is unclear. The current study shows how tree species and pyrolysis temperature (200, 300, 450 and 600 °C) interact to control the physicochemical structure of the PyOM

Pierre-Joseph Hatton and Subhasish Chatterjee have contributed equally to this manuscript.

Responsible Editor: Stuart Grandy.

**Electronic supplementary material** The online version of this article (doi:10.1007/s10533-016-0245-1) contains supplementary material, which is available to authorized users.

P.-J. Hatton · J. A. Bird (⋈)
School of Farth and Environme

School of Earth and Environmental Sciences, Queens College, City University of New York, New York, NY, USA

e-mail: jbird@qc.cuny.edu

P.-J. Hatton · K. J. Nadelhoffer Department of Ecology and Evolutionary Biology, University of Michigan, Ann Arbor, MI, USA

S. Chatterjee  $\cdot$  K. Dastmalchi  $\cdot$  R. E. Stark Department of Chemistry and Biochemistry, City College and CUNY Institute for Macromolecular Assemblies, City University of New York, New York, NY, USA

experimentally derived from <sup>13</sup>C/<sup>15</sup>N-enriched Pinus banksania and Acer rubrum, two important co-occurring gymnosperm and angiosperm tree species from North American boreal-temperate ecotones. Complementary physicochemical and thermodynamic measurements revealed different susceptibilities of the two wood species to charring, with PyOM intermediates formed at lower temperature from the pine, indicating that the tree species regulated the efficacy of PyOM formation. Particularly, we report high-resolution data describing the comprehensive chemical architecture of PyOM (both –C and –N) as they are formed, which are complemented by unique molecular-level insights on their labile fractions. We posit that the tree species and pyrolysis temperature interaction reflects distinctive anatomical features of the two major tree taxa, including greater effective porosity in gymnosperms that promote the loss of volatiles and enhance the heat

#### T. R. Filley

Department of Earth, Atmospheric and Planetary Sciences and the Purdue Climate Change Research Center, Purdue University, West Lafayette, IN, USA

#### A. F. Plante

Department of Earth and Environmental Sciences, University of Pennsylvania, Philadelphia, PA, USA

#### S. Abiven

Department of Geography, University of Zurich, Zurich, Switzerland



exposure of bio-components. This study points to a higher temperature threshold for PyOM production in maple forests compared with pine forests, resulting in potentially more degradable and less sorbtive PyOM in ecotones dominated by the former species.

**Keywords** Char · Black C · Wood · NMR · TMAH

### **Abbreviations**

PyOM Pyrogenic organic matter

JP Jack pine RM Red maple

BET-N<sub>2</sub> SA Brunauer-Emmett-Teller-N<sub>2</sub> surface

area

ssNMR Solid-state nuclear magnetic

resonance

CPMAS Cross polarization-magic-angle

spinning

DPMAS Direct polarization-magic-angle

spinning

MAS Magic-angle spinning

DRIFT Diffuse reflectance infrared Fourier

transmission

<sup>13</sup>C-TMAH <sup>13</sup>C-labeled tetramethylammonium

hydroxide

### Introduction

Forest fires act as a major controller of carbon (C) and nitrogen (N) cycling by releasing gases and contributing pyrogenic organic matter (PyOM or charcoal) to the atmosphere, soils, rivers, and oceans (Masiello and Louchouarn 2013; Randerson et al. 2012). PyOM

X. Gao · C. A. Masiello

Departments of Earth Science, BioSciences, and Chemistry, Rice University, Houston, TX, USA

S. W. Leavitt

Laboratory of Tree-Ring Research, University of Arizona, Tucson, AZ, USA

R. E. Stark

Biochemistry, Biology, Chemistry, and Physics PhD Programs, The Graduate Center of The City University of New York, New York, NY, USA

J. A. Bird

Earth and Environmental Sciences and Biology PhD Programs, The Graduate Center of The City University of New York, New York, NY, USA



aerosols released to the atmosphere likely have a significant net warming effect on the troposphere, even though the impact of these aerosols on climate remains poorly constrained (Bond et al. 2013). Recent data indicate that at least 10 % of dissolved organic C entering the ocean via rivers may be derived from PyOM (Jaffé et al. 2013). In soils, which are a major reservoir for PyOM, PyOM can trigger cascading reactions that alter the functioning of the entire ecosystem in multiple ways that remain hard to predict: PyOM can alter forest C and N biogeochemical cycles (DeLuca et al. 2006; Santin et al. 2015a), microbial communications (Masiello et al. 2013) and activities (Brewer et al. 2014), soil hydraulic conductivity and plant water availability (Barnes et al. 2014).

The PyOM that remains in forest soils can persist for centuries or longer (Gärdenas et al. 2011; Hammes et al. 2010; Schmidt et al. 2011; Singh et al. 2012b). PyOM persistence and reactivity in marine, terrestrial and atmospheric environments are influenced by the physicochemical structure of PyOM, which depends on pyrolysis conditions (Soucémarianadin et al. 2013) and biomass type (McBeath et al. 2014). As such, forest tree composition, depending on the sensitivity and response of fuel types to fires of different intensities (Ryan 2002), may regulate the physical and chemical structure of wood-derived PyOM and, in turn, the ecosystem services they provide (e.g., C sequestration; fertility; water retention and filtering). A better understanding of how wood type and pyrolysis temperature interact to control wood-derived PyOM structure and physicochemical properties is essential to predict the environmental effects of ongoing changes in (i) fire frequency, intensity, severity and distribution (FAO 2010; IPCC 2014) and (ii) tree species composition (Davis and Shaw 2001) on the fate of PyOM contributed to the atmosphere, soils, rivers and oceans.

Wood-derived PyOM undergoes nonlinear physic-ochemical changes with increasing pyrolysis temperature (Hammes et al. 2007; Keiluweit et al. 2010; Knicker 2007, 2008, 2011a; Masiello 2004; Preston and Schmidt 2006). Physical changes occur through shrinking cell structures as the porosity and the surface area increase with pyrolysis temperature (Brewer et al. 2014; Keiluweit et al. 2010; Lehmann 2007; Soucémarianadin et al. 2013). Cellulose and hemicellulose are more readily altered than phenolic and other aromatic constituents as these carbohydrates undergo successive dehydration and aromatization reactions; a

fraction of these constituents is thought to be selectively recombined into amorphous aromatic moieties and further condensed into smaller aromatic units (Keiluweit et al. 2010; Knicker 2011a; Schneider et al. 2010; Soucémarianadin et al. 2013; Wiedemeier et al. 2015). N-containing moieties (e.g., peptide-like compounds) are known to form various aromatic N structures via a great variety of biochemical pathways (Gärdenas et al. 2011; Knicker 2007, 2008, 2011b). Unlike PyOM-C, however, the dynamics of PyOM-N formation remain largely undetermined.

Although initial wood composition controls the dynamics of PyOM formation (Ascough et al. 2008; McBeath et al. 2014; Soucémarianadin et al. 2013), how these dynamics differ between gymnosperm and angiosperm species remains unclear. This work focuses on jack pine (JP; *Pinus banksania*) and red maple (RM; *Acer rubrum*) as representative gymnosperm and angiosperm tree species. We selected JP and RM because they are abundant gymnosperm (Newton 2012) and angiosperm (Barnes 2009) tree species in North American boreal-temperate ecotones that, like boreal-temperate ecotones elsewhere, are particularly vulnerable to climate change (Reich et al. 2015).

This study addresses how wood species and pyrolysis temperature interact to control PyOM formation. We tested the hypothesis that wood source exerts a significant control on PyOM formation, and this control diminishes with temperature. To assess this mechanistic aspect of PyOM formation, our measureincluded intermediate ments temperatures (200-450 °C) that can reveal contrasting susceptibilities of the wood precursors to charring, indicating divergent pyrolysis pathways. We examined the physicochemical structures of <sup>13</sup>C/<sup>15</sup>N-enriched JP and RM sapling stems and PyOM formed at 200, 300, 450 and 600 °C, temperature regimes that are representative of the wildfires occurring in northern fires (Ryan 2002). We used sapling stems to better represent the wood materials most susceptible to form PyOM during wildfires, where PyOM primarily derives from the outermost portion of the woody materials (Santin et al. 2015b). Our investigative approach exploited isotopic enrichment and multi-scale physical approaches in efforts to obtain a comprehensive assessment of PyOM structure and development. We used several complementary analytical techniques to examine the physicochemical structure of <sup>13</sup>C/<sup>15</sup>Nenriched JP and RM materials across the pyrolysis gradient (Fig. S1). We used the isotopic labels to yield exceptionally high-sensitivity <sup>13</sup>C, <sup>15</sup>N and <sup>1</sup>H solidstate nuclear magnetic resonance (ssNMR) to determine (supra)molecular organization in the PyOM. To complement this spectroscopic approach, we used <sup>13</sup>Clabeled tetramethylammonium hydroxide thermochemolysis (<sup>13</sup>C-TMAH) to quantify hydrolysable compounds, which we hypothesize to be the most environmentally reactive (labile) forms of aromatic and aliphatic PyOM (Filley et al. 2006). We examined yields and reactions of aromatization and condensation (C, H, O, N), as well as losses of cellulose relative to lignin (18O) to better understand PyOM formation pathways. We used pycnometry, Brunauer-Emmett-Teller (BET)-N2 surface area (SA), and diffuse reflectance infrared Fourier transmission (DRIFT) to characterize changes in physical properties including density, porosity, SA, and typical functional moieties. Finally, we conducted simultaneous thermogravimetry (TG), differential scanning calorimetry (DSC) and evolved gas analysis (EGA) experiments to characterize thermodynamic stabilities and energy contents.

#### Materials and methods

#### Production

We made <sup>13</sup>C/<sup>15</sup>N-enriched PyOM from commercially-available JP (1y-old) and RM (2y-old) saplings labeled as described by Bird and Torn (2006), using <sup>13</sup>CO<sub>2</sub> and <sup>15</sup>NH<sub>4</sub>SO<sub>4</sub> for JP and <sup>13</sup>CO<sub>2</sub>, <sup>15</sup>NH<sub>4</sub>Cl and K<sup>15</sup>NO<sub>3</sub> for RM (the <sup>15</sup>N forms applied varied with the preferred N form for each tree species). We pyrolyzed ~2 cm-long pieces of air-dried stems (with bark) for 5 h under N<sub>2</sub> at 200, 300, 450 and 600 °C as described by and using the same equipment as in Hammes et al. (2006) to produce 11–30 g of each sample type. PyOM samples are referred to as JPXXO and RMXXO or PyOMXXO, with XXO indicating the pyrolysis temperature. Details are found in the Supporting Information.

### Elemental and isotopic composition

We extracted JP and RM cellulose using the Jayme—Wise oxidation method (Leavitt and Danzer 1993). Proximate C fractions were separated as described by Ryan et al. (1990). We measured C and N content



using a 4010 CHN gas analyzer (Costech Analytical Tech., Valencia, CA); <sup>13</sup>C and <sup>15</sup>N isotope ratios using a PDZ Europa elemental analyzer interfaced to a Sercon 20-20 isotope ratio mass spectrometer (IRMS; Sercon Ltd., Cheshire, UK); H elemental concentration using a high temperature elemental analyzer (Hekatech, Wegberg, DE); and O elemental and isotopic composition using a PYROcube (Elementar Analysensysteme, Hanau, DE) interfaced to a Sercon 20-20 IRMS (Sercon Ltd., Cheshire, UK).  $\delta^{18}$ O were expressed with respect to Vienna Standard Mean Ocean Water.

# Pycnometry

We measured skeletal density (mass/volume excluding accessible pores) and envelope density (mass/total pore volume) as described by Brewer et al. (2014). We measured skeletal density using an AccuPyc II 1340 gas displacement analyzer fitted with a 1 cm³ chamber (Micromeritics, Norcross, GA). We measured envelope density using a GeoPyc 1360 envelope density analyzer (Micromeritics, Norcross, GA) using DryFlo® as displacement medium. We calculated porosity as 1—(skeletal density/envelope density).

### BET-N<sub>2</sub> SA

We measured SA using a Quantachrome Autosorb-3b Surface Analyzer located within the Rice University Shared Equipment Authority. We used air-dried wood; PyOM200 and PyOM300 vacuum-dried overnight at +60 °C; PyOM450 and PyOM600 vacuum-dried overnight at +200 °C. We obtained  $N_2$  adsorption/desorption isotherms at 77°K by a 26-point analysis for relative pressures P/P<sub>0</sub> from  $1.21 \times 10^{-4}$  to 0.99.

### Thermal analyses

We measured simultaneous TG, DSC and evolved gas analysis (EGA) according to Fernández et al. (2012). We subjected samples equivalent to  $\sim 4$  mg C to ramped combustion to 700 °C at 10 °C min<sup>-1</sup> in an oxidizing atmosphere, and analyzed using a STA 409PC Luxx simultaneous thermal analyzer (Netzsch-Gerätebau GmbH, Selb, Germany) coupled to a LI-840 CO<sub>2</sub>/H<sub>2</sub>O infrared gas analyzer (IRGA, LI-COR Biosciences, Lincoln NE, USA). We calculated the

thermal indices (i.e., energy content, energy density,  $TG-T_{50}$ ,  $DSC-T_{50}$ , and  $R_{50}$ ) as described by Fernández et al. (2012) and Harvey et al. (2012).

# <sup>13</sup>C. <sup>15</sup>N. and <sup>1</sup>H ssNMR

We acquired and referenced NMR spectra according to Chatterjee et al. (2012). We used a 4-channel Agilent (Varian) DirectDrive 1 (VNMRS) spectrometer (150 MHz <sup>13</sup>C, 60 MHz <sup>15</sup>N; 600 MHz <sup>1</sup>H; Agilent Technologies, Santa Clara, CA, USA) to conduct both <sup>13</sup>C cross polarization–magic-angle spinning (CPMAS) and direct polarization-magic angle spinning (DPMAS) experiments. The spectrometer was equipped with a 1.6 mm HXY fastMAS probe in which  $\sim 5$  mg samples were spun at  $30 \pm 0.02$  kHz. We obtained ramped-amplitude  $^{13}$ C CPMAS spectra using a <sup>13</sup>C field strength corresponding to  $\sim 80$  kHz and a <sup>1</sup>H field strength that was varied linearly by 10-20 % (Metz et al. 1994). We achieved high-power heteronuclear <sup>1</sup>H decoupling 170-185 kHz using the SPINAL pulse sequence (Fung et al. 2000). For PyOM300, CPMAS <sup>13</sup>C measurements with interrupted proton decoupling for periods of 10-40 µs prior to signal acquisition were also conducted at 10 kHz MAS. We used <sup>13</sup>C DPMAS measurements of wood, PvOM300 and PvOM450 to estimate the degree of aromatization [(0-90 or 0-110 ppm)/(90-160 or 110-165 ppm)] (Serra et al. 2014; Soucémarianadin et al. 2014). We performed <sup>15</sup>N CPMAS measurements with CP times of 0.1-1.0 ms, 15 kHz spinning rate, 1 s recycle delay between acquisitions and a 10-20 % linear ramp of the <sup>1</sup>H field strength. We assessed reproducibility from replicate <sup>15</sup>N spectra of PyOM300 and PyOM450. We acquired <sup>1</sup>H MAS spectra with a 6 s recycle delay and 36 kHz MAS. Details are found in the SI.

# <sup>13</sup>C-TMAH

We measured the composition and concentration of substituted fatty acids, phenols, and lignin monomers extractable by thermally-assisted hydrolysis and methylation as described by Filley et al. (2006). Into a 3  $\times$  3 mm platinum boat, we weighed 100–300  $\mu$ g of sample and then 4  $\mu$ L of  $^{13}$ C-TMAH solution (Filley et al. 1999). The mixture sat at room temperature under a He atmosphere for 5 min before in-line thermochemolysis (at 350 °C) using a Shimadzu



Pyr-4a pyrolysis unit on a Shimadzu (Kyoto, Japan) GC17A interfaced to a Shimadzu QP5050A quadrupole mass spectrometer. The chromatographic separation of extractable compounds was performed using a fused silica column (Restek RTx-5, 30 m, 0.25 mm, 0.25  $\mu m$ ); temperature ramped from 60 to 300 °C at 7 °C min $^{-1}$  and maintained at 300 °C for 15 min. The injector base of the Pyr-4a was maintained at 320 °C (25/1 injection split ratio).

### Results

# Elemental and isotopic composition

JP and RM samples lost  $\sim 55$  % of C,  $\sim 94$  % of O and  $\sim 91$  % of H across the pyrolysis temperature gradient (Table 1); RM lost 62 % of N versus 53 % for JP. More than 75 % of the losses in C, H, O and N occurred between 200 and 450 °C for both species. Decreases in natural  $^{18}$ O abundance, relative elemental contents, and H/C and O/C atomic ratios showed that this temperature threshold was reached at lower temperature for JP than for RM. Despite drastic changes in both C and N content,  $^{13}$ C and  $^{15}$ N enrichments remained comparatively stable across the

pyrolysis gradient, suggesting a uniform labeling of the wood precursors.

### Physical properties

Porosity increased non-linearly across the pyrolysis gradient for both JP and RM, mostly between 200 and 450 °C, stemming from an increase in skeletal density with a concomitant decrease in envelope density (Table 1). BET–N<sub>2</sub> SA of both species increased exponentially with temperature (Table 1;  $R^2 \geq 0.77$ ), especially >450 °C.

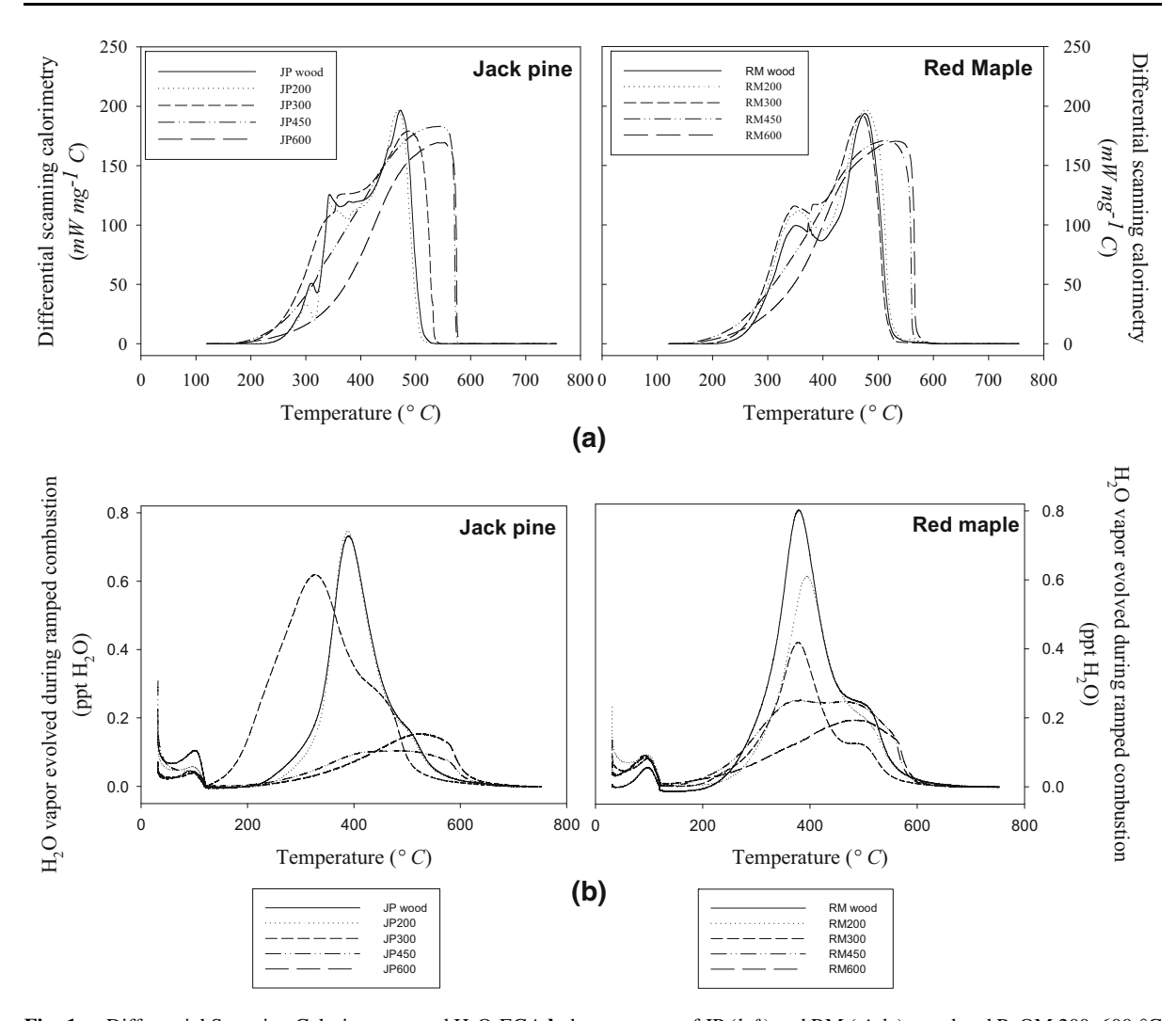
# Thermal stability

DSC thermograms of JP and RM (Fig. 1a) showed the progressive alteration of wood components such as cellulosic and phenolic structures (loss of peaks at  $\sim 350$  and  $\sim 450$  °C, respectively), and the formation of thermally more stable materials >450 °C (peak at  $\sim 550$  °C). Most of the increases in (i) energy content (i.e., amount of energy per unit of mass; >69 %), (ii) energy density (i.e., amount of energy per unit of C; >78 %), (iii) DSC-T<sub>50</sub> (i.e., temperature at which half of the heat is released; >50 %), (iv) TG-T<sub>50</sub> (i.e., temperatures at which half of the mass is lost (>83 %),

**Table 1** Yield, elemental and isotopic composition and physical properties of JP and RM cellulose, wood and PyOM 200–600  $^{\circ}$ C (N = 3)

Sample	Yield	С	N	О	Н	C/N	H/C	O/C	<sup>13</sup> C	<sup>15</sup> N	$\delta^{18}O$	Skeletal	Envelope	Porosity	BET-N <sub>2</sub>
	% of initial	$g kg^{-1}$				Mass ratio	Atomic ratio		Atom %		‰	density g cm <sup>-3</sup>	density	%	${\rm SA} \atop {\rm m}^2 {\rm g}^{-1}$
JP cellulose	22	430	_	538	57	_	1.6	0.9	2.55	_	30.4	_	_	_	-
JP wood	100	464	2.8	470	54	165	1.4	0.8	2.20	19.2	24.1	1.38	0.51	63	2.6
JP200	83	507	3.4	496	55	147	1.3	0.7	2.42	18.8	24.6	1.38	0.55	60	2.8
JP300	45	669	5.4	286	46	124	0.8	0.3	2.37	18.8	20.8	1.33	0.33	75	4.3
JP450	27	786	5.4	197	29	146	0.4	0.2	2.33	18.9	15.2	_	_	_	13
JP600	25	831	5.3	100	20	156	0.3	0.1	2.31	18.8	8.2	1.55	_	_	212
RM cellulose	26	423	_	533	57	_	1.6	0.9	3.49	_	29.5	_	_	_	_
RM wood	100	451	6.4	492	53	70	1.4	0.8	3.81	8.9	24.4	1.41	0.56	60	0.5
RM200	87	495	6.9	517	53	72	1.3	0.8	3.76	8.9	23.8	1.38	0.55	61	1.4
RM300	51	574	9.0	369	49	64	1.0	0.5	3.74	8.9	24.6	1.41	0.39	72	2.3
RM450	28	761	9.4	188	26	81	0.4	0.2	3.85	9.1	15.5	1.49	0.33	78	3.3
RM600	26	795	9.5	120	20	84	0.3	0.1	3.90	9.2	13.2	1.61	0.31	81	132





 $\textbf{Fig. 1} \quad \textbf{a} \ \text{Differential Scanning Calorimetry } \textbf{a} \ \text{and} \ H_2\text{O-EGA} \ \textbf{b} \ \text{thermograms of JP} \ (\textit{left}) \ \text{and} \ \text{RM} \ (\textit{right}) \ \text{wood and PyOM 200-600} \ ^{\circ}\text{C}$ 

and (v) recalcitrance index  $R_{50}$  (TG- $T_{50, sample}$ /TG- $T_{50, graphite}$ ; >83 %) occurred between 200 and 450 °C for both JP and RM (Table S1), revealing the formation of energy-rich structures (Kuo et al. 2008; Zimmermann 2010). Differences in the extent of the increase in energy content, energy density, and DSC- $T_{50}$  of RM versus JP across the pyrolysis gradient revealed a pattern of thermodynamic changes occurring at lower pyrolysis temperature for JP than for RM. This comparison was also evident from the thermograms, which showed that JP300 was substantially affected by pyrolysis whereas RM300 was not.

 $H_2O$ -EGA thermograms (Fig. 1b) showed the loss of free and non-structural water (i.e., drying and adsorbed water; peak at  $\sim 100$  °C) and structural

water from thermodynamically more stable structures (Harvey et al. 2012), such as cellulose (peak at  $\sim 380$  °C) and phenols (peak at  $\sim 560$  °C), via various concurrent dehydration reactions (Scheirs et al. 2001). The amount of structural water lost declined with increasing PyOM pyrolysis temperature for both wood sources, but more readily so for JP than RM. The increase in the energy required to extract structural water for PyOM >450 °C implicates the formation of thermally more stable structures.

### Comprehensive chemical architecture

JP and RM ssNMR spectra showed the progressive thermal alteration of wood components, the



subsequent formation of an increasing proportion of disordered C and N aromatics across the pyrolysis gradient, more facile charring of the JP (JP300 is thermally altered more significantly than RM300) and the presence of heat-resistant aliphatics ≥450 °C. The uniform isotopic enrichments across the pyrolysis gradient ensured unbiased representation of the chemical compounds present in each PyOM sample as viewed by both ssNMR and <sup>13</sup>C-TMAH measurements.

JP and RM wood C moieties (Fig. 2) displayed <sup>13</sup>C NMR resonances that were identified according to the main categories of alkyl chain groups (–CH<sub>2</sub>CH<sub>3</sub>, 0–45 ppm), oxygenated alkyls (-CH<sub>n</sub>O, 45–110 ppm), alkenes and arenes (–CH = CH, 110–160 ppm), and carbonyls (–C = O, 160–220 ppm), reflecting cellulose, hemicellulose, lignin, and wax constituents (Baldock and Smernik 2002; Chatterjee et al. 2012; Hammes et al. 2006; McBeath and Smernik 2009; Smernik et al. 2002; Solum et al. 1995; Soucémarianadin et al. 2013). No discernible changes were found between the wood source and PyOM200 for either species.

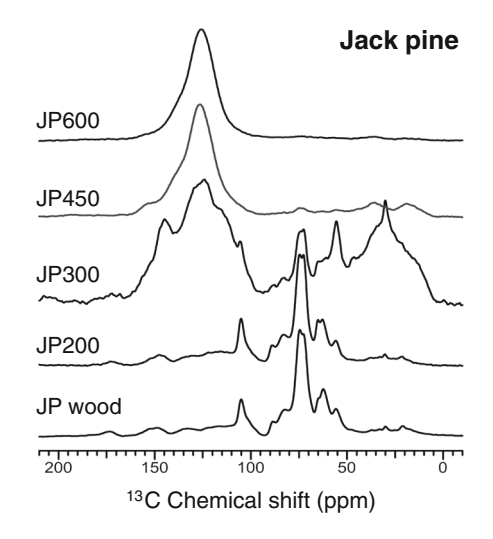
While RM300 showed moderate broadening of peaks in the  $-\text{CH}_2\text{CH}_3$  region and the appearance of a new aromatic spectral envelope ( $\sim 125$  ppm), JP300 showed broad spectral features in both aliphatic and aromatic regions. The aliphatic chain carbons in JP300 were dominant compared with the polysaccharide CH<sub>2</sub>O and CHO groups displayed in JP  $^{13}\text{C}$  wood spectra acquired with either cross polarization (CP; Fig. 2) or direct polarization (DP; Fig. S2), supporting

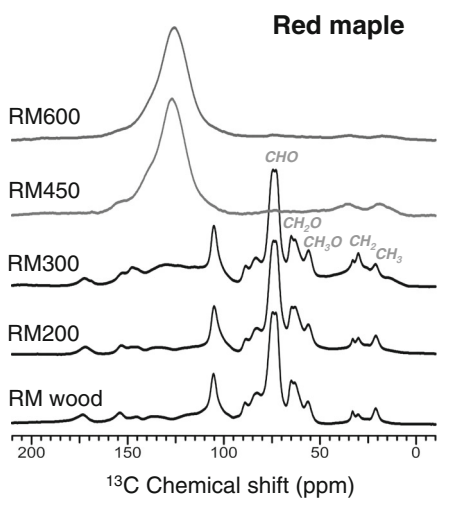
the facile polysaccharide depolymerization of this plant biomass that has been proposed to occur at an intermediate pyrolysis temperature (Keiluweit et al. 2010). The broad resonances in the aromatic regions are attributable to structural heterogeneity of the disordered PyOM materials or the presence of paramagnetic species (Chatterjee et al. 2012; Wind et al. 1993).

Both JP450 and RM450 showed nearly complete absence of the polysaccharides and retention or formation of a prominent broad aromatic <sup>13</sup>C resonance, though small peaks remained visible from oxygenated aryl and chain alkyl moieties. JP600 and RM600 both showed a single broad aromatic <sup>13</sup>C signal that obscures structural detail regarding plausible transformations (such as complete removal of lignaceous constituents); small aliphatic signals were evident, particularly for RM600. DRIFT spectra (Fig. S5) corroborated the ssNMR data, showing the progressive loss of wood polysaccharides <450 °C and the presence of thermally-formed aromatic structures ≥450 °C. The formation of disordered C aromatics and the greater thermal sensitivity of JP compared with RM were confirmed by DP magicangle spinning (MAS) <sup>13</sup>C spectra (Fig. S2) and computed degrees of aromatization (Table S3).

<sup>1</sup>H MAS spectra (Fig. 3) corroborated the contributions of disordered aromatics and revealed the persistence of heat-resistant aliphatics in PyOM ≥450 °C. MAS at 36 kHz appears sufficient to yield observable spectral features for each of the PyOM samples, but the small chemical shift

Fig. 2 150 MHz CPMAS <sup>13</sup>C NMR spectra obtained with 30 kHz MAS from <sup>13</sup>C/<sup>15</sup>N-enriched JP (*left*) and RM (*right*) wood and PyOM 200–600 °C. The <sup>13</sup>C NMR chemical shifts were assigned to the main categories of alkyl chain groups (0–45 ppm), oxygenated alkyls (45–110 ppm), alkenes and arenes (110–160 ppm), and carbonyls (160–220 ppm)







dispersion of the aliphatic constituents produced overlapped resonances that appeared at  $\sim 2-4$  ppm. For PyOM ≥300 °C, additional contributions from aromatic functional groups were at  $\sim$  7.2 ppm. The aliphatic resonance narrowed further, displayed a shoulder, and was then represented prominently in the spectrum as reported earlier for ponderosa pine wood pyrolyzed at 450 °C (Chatterjee et al. 2012). Whereas motional narrowing of the alkyl <sup>1</sup>H resonances was expected from our prior study (Chatterjee et al. 2012), the observation of wellresolved aryl <sup>1</sup>H resonances could also reflect the presence of fused aromatic ring structures that contain chemically dilute <sup>1</sup>H nuclei, resulting in diminished <sup>1</sup>H-<sup>1</sup>H dipolar couplings and less spectral broadening. Support for this hypothesis of sparse aryl hydrogens comes from delayed decoupling <sup>13</sup>C spectra (Fig. S3), which showed retention of the aromatic signal intensity.

<sup>15</sup>N CPMAS spectra of JP and RM wood displayed a major resonance at 120 ppm (amides or pyrroles) and a minor resonance at 74 ppm (secondary amines; Fig. 4). The amine peak, which is more discernible for the RM species, was diminished in relative intensity for PyOM200. Pyrolysis caused the appearance of new downfield resonances (at ∼160 and ∼170 ppm; arenes), and the envelope of resonance intensity became broader (50–60 ppm). PyOM300 spectra showed preferential retention of the 120 ppm signal for RM300, confirming the relatively greater thermal resistance of RM compared with JP. Both JP and RM samples showed a sharper slowly-polarizing resonance at 120 ppm and a rapidly polarizing, broader resonance at ∼140 ppm (Fig. S4); the broader feature

at  $\sim$  140 ppm predominated  $\geq$  450 °C. This appearance of new broadened signals with altered chemical shifts suggests the presence of chemically transformed N moieties in the PyOM rather than retention of nitrogenous structures that were present in the precursor wood.

### Hydrolysable constituents

Hydrolysable lignin phenols, non-lignin phenols (e.g., demethylated lignin and tannins), and normal and substituted fatty acids were revealed by <sup>13</sup>C-TMAH thermochemolysis, and displayed yields and compositions that were species and temperature dependent (Table 2), with concentrations dropping with increasing pyrolysis temperature but to very different degrees depending on the wood source. These compounds extracted by the thermochemolysis procedure are more easily liberated than those requiring C–C breakage by higher temperature analytical pyrolysis methods, and thus represent potentially more metabolizable or leachable structures within the sample.

Wood precursors differed in potentially reactive phenols (lignin and non-lignin aromatic hydrocarbons) and with respect to fatty acid yields and compositions: RM wood was substantially richer than JP wood in hydrolysable lignin ( $\times 1.6$ ), non-lignin phenols ( $\times 3.0$ ) and fatty acids ( $\times 1.7$ ). RM also exhibits a higher proportion of syringyl to guaiacyl lignin phenols, which differ in the degree of methoxyl substitution and potential crosslinking: syringyl-based lignin with higher methoxyl content has a lower degree of cross-linked structures. The differences

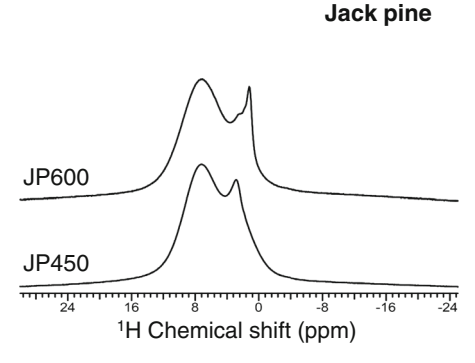
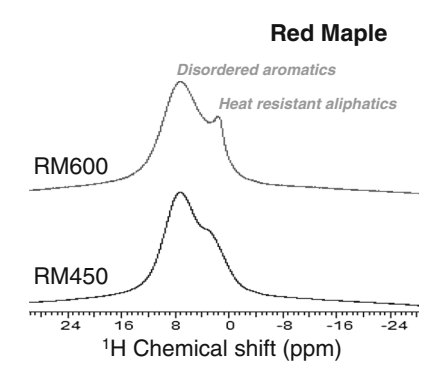
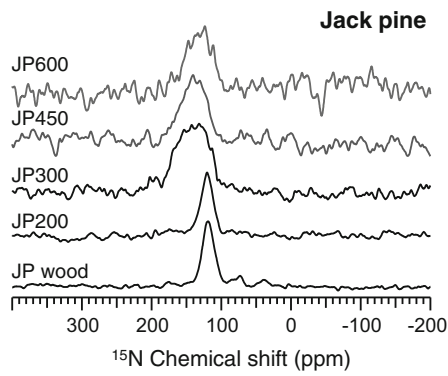


**Fig. 3** 600 MHz <sup>1</sup>H NMR spectra obtained with 36 kHz MAS for <sup>13</sup>C, <sup>15</sup>N-enriched chars from <sup>13</sup>C/<sup>15</sup>N-enriched JP (*left*) and RM (*right*) PyOM 450 and PyOM 600 °C. The <sup>1</sup>H NMR



chemical shifts were assigned to aliphatics (2–4 ppm) and aromatic moieties ( $\sim$  7.2 ppm)





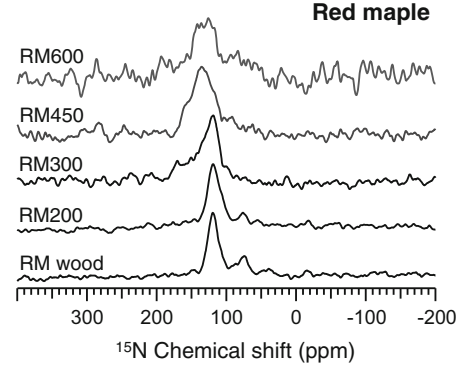


**Fig. 4** 60 MHz CPMAS <sup>15</sup>N NMR spectra obtained with a contact time of 300 μs and 15 kHz MAS from <sup>13</sup>C/<sup>15</sup>N-enriched JP (*left*) and RM (*right*) wood and PyOM 200–600 °C. The <sup>15</sup>N

NMR chemical shifts were assigned to amides or pyrroles (120 ppm), secondary amines (74 ppm), and arenes (140–170 ppm)

**Table 2** <sup>13</sup>C-TMAH extractable phenols and fatty acids from JP and RM wood and PyOM 200–600 °C (N = 2)

	Lignin phe	enols		Non-lignin phenols	Fatty acids	
	G-type mg g <sup>-1</sup> we	S-type ood source C	C-type			
JP wood	26.5	0.39	2.9	21.2	14.6	
JP200	22.9	0.36	2.4	18.3	15.8	
JP300	2.2	0.05	0.35	5.9	12.7	
JP450	0.03	0.01	_	0.09	0.07	
JP600	0.07	_	0.003	3.30	_	
RM wood	21.2	23.4	2.3	63.1	25.4	
RM200	13.5	15.8	1.3	36.9	13.4	
RM300	4.8	6.8	0.5	14.3	7.7	
RM450	0.01	0.01	_	0.62	0.08	
RM600	0.01	0.003	_	0.01	0.04	

Lignin G, S and C-types are for Guaiacyl, Syringyl and Ciannamic acid, respectively

between JP and RM woods persisted across the pyrolysis gradient, with very few recognizable compounds extractable >450 °C for either species. Below 450 °C, JP and RM hydrolysable compounds showed distinct loss behaviors, with RM compounds altered more gradually than JP. For JP,  $\sim 71$  % of the total losses of hydrolysable lignin and non-lignin phenols occurred between 200 and 300 °C, whereas 76 % of the total losses of hydrolysable fatty acids occurred between 300 and 450  $^{\circ}$ C. In contrast, 38, 35 and 24 %of the total losses of hydrolysable RM lignin and nonlignin phenols occurred at the three pyrolysis temperatures <450 °C; the total losses of hydrolysable fatty acids were 46, 25 and 26 %. Although RM and JP share essentially the same range of chemicals released, i.e., 28/41 phenols (Table S4) and 15/22 fatty acids (Table S5), the loss patterns of hydrolysable compounds appear species-specific for each class of compounds.

# Discussion

In North American boreal-temperate ecotones, predicted changes in forest tree species composition (Davis and Shaw 2001) and in both fire frequency and intensity (FAO 2010; IPCC 2014) may result in relatively more PyOM derived from RM (angiosperm) and less from JP (gymnosperm). Here, we used an information-rich strategy in which assessments of structural integrity and supramolecular order were complemented by molecular-scale spectroscopic measurements. This approach incorporates and extends experimental methods used previously for soil organic



matter, whereby selective generation of molecular fragments by <sup>13</sup>C-TMAH methods was reported in combination with global solid-state <sup>13</sup>C NMR structural characterization (Chefetz et al. 2000). We demonstrate that even though high-temperature PyOM (>450 °C) displayed comparable spectroscopic and structural signatures for JP and RM, measurements at the intermediate temperatures revealed distinctive susceptibilities of the two types of wood to charring and thus contrasting pyrolysis pathways for both PyOM-C and -N. Such a strong wood species-bypyrolysis temperature interaction on PyOM properties suggests that predicted changes in fuel types could alter PyOM environmental reactivity, with potential implications for C and N biogeochemistry and ecosystem services (e.g., C sequestration; fertility; water retention and filtering; etc.).

Wood species controls the efficacy of PyOM formation

We report converging lines of evidence for the more facile charring of JP than RM  $\leq$ 450 °C. This finding suggests that the wood precursor regulates the efficacy of PyOM formation differently for RM (angiosperm) and JP (gymnosperm).

Wood source determined heat-resistance ≤450 °C through the interaction of physical and chemical properties. The modest differences in wood chemical composition are in sharp contrast to their pyrolytic behaviors <450 °C. Proximate C (Table S6), DSC thermograms, NMR and DRIFT data (Fig. S5) revealed only minor compositional differences between the wood precursors in terms of cellulosic and lignin-based (ARF) compound proportions. Thermal analyses of model cellulose (Wang et al. 2013), hemicellulose (Werner et al. 2014), lignin (Bredu and Vasile 2010) and ligno-cellulosic mixtures (Giudicianni et al. 2013) further suggest that differences in initial composition alone cannot explain the striking differences we observed in PyOM formation. <sup>13</sup>C-TMAH data revealed that the same individual (hydrolysable) compounds showed very different patterns of thermal alteration depending on the wood source, further suggesting that the molecular composition alone does not explain the differences in PyOM formation and potential environmental reactivity between the two studied species. Thus, either minor changes in fractions including non-polar and water soluble extractives (Table S6), which exhibit the greatest difference between the sources, have a disproportionately large effect with respect to their content in each wood source, or other factors, such as ultrastructural/anatomical differences are controlling charring pathways.

Concomitantly, BET-N<sub>2</sub> SA measurements showed greater SA for JP wood than for RM wood. Similar pore spaces suggest greater micropore volumes for JP than RM (Brewer et al. 2014). This SA difference can be attributed to the distinct anatomical arrangements that exist for these angiosperm and gymnosperm species, e.g., cell size (small gymnosperm tracheids versus generally larger angiosperm vessels) and connectivity (lower end-wall resistance for gymnosperm compared with angiosperm conduits) (Sperry et al. 2006). We posit that such anatomical differences may explain the contrasting degrees of heat-resistance for JP and RM components, by controlling (i) the effective porosity and connectivity that allows for escape of the volatiles and (ii) the surface exposure to heat, i.e., heat-exposure of bio-components, and thus their apparent activation energy (Di Blasi 2008). Support for this hypothesis comes from model biopolymer pyrolysis studies showing the interactive effects of wood physical and chemical properties on the mechanisms and the pathways of PyOM formation (Beaumont and Schwob 1984). Future work will be required to evaluate if our results can be extended more widely to angiosperm- and gymnosperm-specific anatomical features.

The influence of the wood source on PyOM persisted >450 °C. NMR, DRIFT (Fig. S5) and <sup>13</sup>C-TMAH measurements revealed no discernible influence of the wood source on PyOM >450 °C. However, condensation indices of the primarily thermally-induced aromatic structures, i.e., relative C contents, BET-N<sub>2</sub> SA and natural <sup>18</sup>O signatures, suggest that JP is more readily condensed than RM. This view is supported by the thermograms, which show that PyOM600 is thermodynamically more stable than PyOM450.

Temperature is the necessary driver of PyOM formation

Our data support the claim that pyrolysis temperature is a strong controlling factor on the structure of the PyOM (Chatterjee et al. 2012; Keiluweit et al. 2010;



Soucémarianadin et al. 2013). Both RM and JP, chosen as typical angiosperm and gymnosperm tree species from North American temperate-boreal ecotones, showed non-linear thermal alterations and a temperature threshold for aromatization reactions between 200 and 450 °C.

Dehydration and thermal alteration of several wood components occur at 200 °C. The loss of non-structural water was evident from H/C and O/C ratios, natural <sup>18</sup>O signatures and H<sub>2</sub>O thermograms, supporting earlier reports for low-temperature wood-derived PyOM (Baldock and Smernik 2002; Hammes et al. 2006; Harvey et al. 2012; Scheirs et al. 2001). Modest losses of thermodynamically labile cellulosic compounds and substantial losses of potentially reactive fatty acids, lignin and non-lignin phenols were also observed after pyrolysis at 200 °C. These findings extend existing knowledge on the thermal degradation of model wood cellulose, hemicellulose and lignin (Beall and Eickner 1970; Bredu and Vasile 2010) to entire wood stems.

Substantial losses and selective aromatization reactions occurred between 200 and 450 °C. Major changes in PyOM physicochemistry were evident from converging thermodynamic, elemental, molecular and supramolecular evidence. Changes in yields and relative elemental concentrations are typical of progressive volatilization as well as dehydration and aromatization reactions (Hammes et al. 2006; Keiluweit et al. 2010; Knicker 2007, 2011b; Wiedemeier et al. 2015), resulting in thermodynamically more stable entities. Carbon to N ratios were comparable to those reported for other wood-derived PyOM (Santos et al. 2012; Soucémarianadin et al. 2013), and they suggest that C and N moieties were similarly affected by pyrolysis temperature. The progressive shift of natural <sup>18</sup>O values from cellulose-like to lignin-like signatures (Gray and Thompson 1977) that we observed for both species across a gradient of pyrolysis temperatures could be attributed to a more facile dehydration, loss of cellulose-like components or preferential transformation of lignin-like constituents into progressively more condensed structures (Chatterjee et al. 2012). DSC thermograms and DRIFT spectra (Fig. S5) also indicated substantial losses in cellulose, followed by the thermal alteration of phenolic compounds and their selective recombination into thermodynamically more stable aromatic structures. This is corroborated by a substantial decline in the amount and the increase in (combustion) temperature at which structural water was extracted from PyOM between 200 and 450 °C. Thermochemolysis and NMR data support and extend these findings, showing (i) the substantial loss of polysaccharides and fatty acids between 200 and 450 °C, (ii) the retention of traces of wood-derived compounds and (iii) the formation or modification of disordered (or amorphous) C and N aromatics after pyrolysis at 450 °C. Furthermore, <sup>1</sup>H MAS NMR spectra indicate the presence of a population of alkyl groups and proton-deficient aromatic PyOM components that are mobile on the NMR time scale, making them potentially susceptible to 13C-TMAH thermochemolysis. These findings also strengthen earlier reports (Chatterjee et al. 2012; Knicker 2007). Possible mechanisms for C and N aromatic formation were reviewed by Knicker (2007) and by Bredu and Vasile (2010). Our results showed concomitant changes in PyOM physical structure, with shrinking cells and increasing porosity and SA also observed previously (Brewer et al. 2014; Keiluweit et al. 2010).

Condensation of the thermally formed, disordered aromatics occurred >450 °C (Brewer et al. 2014; Wiedemeier et al. 2015). The <sup>13</sup>C-TMAH and NMR offered no clear evidence for a greater degree of condensation for PyOM600 than for PyOM450. Following Wiedemeier, et al. (2015), the increase in relative C contents, skeletal density and SA indicated the condensation of the aromatic structures >450 °C. This view is supported by natural <sup>18</sup>O signatures at or below those previously reported for lignin (Gray and Thompson 1977). Both CO<sub>2</sub> and H<sub>2</sub>O thermograms also showed that PyOM600 are thermodynamically more stable than PyOM450 despite remaining traces of heat-resistant components.

### Implications for environmental sciences

Predicted shifts in tree species ranges (Davis and Shaw 2001) could constrain JP habitats (Newton 2012) and favor RM expansion (Barnes 2009) to forests in North American temperate-boreal ecotones (Reich et al. 2015). In addition, predicted increases in temperature and drought frequency could result in more frequent and more intense forest fires (FAO 2010; IPCC 2014), further accelerating changes in tree distribution ranges. Herein, our results suggest that such shifts in fuel type from JP (gymnosperm) to RM (angiosperm) could affect the environmental properties of the PyOM



contributed to the atmosphere, the soils and the hydrosphere, with potential implications for C and N biogeochemistry and ecosystem services (C sequestration; fertility; water retention and filtering).

Considering the interactive effects of wood type and pyrolysis temperature on PyOM structure will substantially improve current estimates of PyOM persistence and reactivity potentials in North American forest soils. Following Harvey et al. (2012) and Singh et al. (2012a), our thermal  $R_{50}$  indices and degrees of C aromatization (estimated by DPMAS <sup>13</sup>C NMR and DRIFT) both suggest that RM-derived PyOM are more degradable than JP-derived PyOM. This is in agreement with the <sup>13</sup>C-TMAH data showing more potentially hydrolysable compounds for RM than JP. Our results suggest that shifts in fuel type from JP (gymnosperm) to RM (angiosperm) will result in a greater contribution of more degradable and less sorbtive PyOM. Our results can be scaled up to the landscape level to provide more comprehensive assessments of PyOM stocks and reactivity under current and future climate conditions in North American forests. Future work will have to assess how changing tree species composition will affect natural PyOM yields by elucidating the interaction between forest tree composition affects and fire severity.

Acknowledgments This research was supported by the National Science Foundation (DEB-1127253). The NMR resources were supported by The City College of New York (CCNY) and the CUNY Institute of Macromolecular Assemblies, with infrastructural assistance provided by the National Institutes of Health through the National Institute on Minority Health and Health Disparities (8G12 MD007603). We are grateful to F. Santos for growing the RM, B. Dewey for performing the proximate C analyses and to the UC Davis Stable Isotope Facility for isotope analyses. We thank the anonymous reviewers for their constructive comments.

**Author Contributions** JAB, TRF and KJN conceived and designed the study. PJH analyzed the data and was the primary author of the manuscript. RES and SC designed the NMR experiments, which were performed and analyzed by SC, KD, and RES. TRF did the <sup>13</sup>C-TMAH measurements. AFP did the thermal analyses. SA did the DRIFT measurements. XG and CM did the pycnometry and SA measurements. SL did the cellulose extractions. The manuscript was written through contributions of all authors. All authors contributed to interpreting the data and editing the manuscript. All authors have given approval to the final version of the manuscript.

**Funding Sources** National Science Foundation (DEB-1127253).

#### References

- Ascough PL, Bird MI, Wormald P, Snape CE, Apperley D (2008) Influence of production variables and starting material on charcoal stable isotopic and molecular characteristics. Geochim Cosmochim Acta 72:6090–6102
- Baldock JA, Smernik RJ (2002) Chemical composition and bioavailability of thermally, altered pinus resinosa (red pine) wood. Org Geochem 33:1093–1109
- Barnes BV (2009) Tree response to ecosystem change at the landscape level in Eastern North America. Forstarchiv 80:76–89
- Barnes RT, Gallagher ME, Masiello CA, Liu Z, Dugan B (2014) Biochar-induced changes in soil hydraulic conductivity and dissolved nutrient fluxes constrained by laboratory experiments. PLoS One 9(9):e108340
- Beall FC, Eickner HW (1970) Thermal degradation of wood components: a review of the literature. In: USDA Forest service (ed) FLP 130, p 1–29
- Beaumont O, Schwob Y (1984) Influence of physical and chemical parameters on wood pyrolysis. Ind Eng Chem Res 23:627
- Bird JA, Torn MS (2006) Fine roots versus needles: a comparison of <sup>13</sup>C and <sup>15</sup>N dynamics in a ponderosa pine forest soil. Biogeochemistry 79(3):361–382
- Bond TC, Doherty SJ, Fahey DW, Forster PM, Berntsen T, DeAngelo BJ, Flanner MG, Ghan S, Karcher B, Koch D, Kinne S, Kondo Y, Quinn PK, Sarofim MC, Schultz MG, Schultz M, Venkataraman C, Zhang H, Zhang S, Bellouin N, Guttikunda SK, Hopke PK, Jacobson MZ, Kaiser JW, Kilmont Z, Lohmann U, Schwarz JP, Schindell D, Storelvmo T, Warren SG, Zender CS (2013) Bounding the role of black carbon in the climate system: a scientific assessment. J Geophys Res Atmos 118:5380–5552
- Bredu M, Vasile C (2010) Thermal alteration of lignin—a review. Cellul Chem Technol 44(9):353–363
- Brewer CE, Chuang VJ, Masiello CA, Gonnermann H, Gao X, Dugan B, Driver LE, Panzacchi P, Zygourakis K, Davies CA (2014) New approaches to measuring biochar density and porosity. Biomass Bioenergy 66:176–185
- Chatterjee S, Santos F, Abiven S, Itin B, Stark RE, Bird JA (2012) Elucidating the chemical structure of pyrogenic organic matter by combining magnetic resonance, midinfrared spectroscopy and mass spectrometry. Org Geochem 51:35–44
- Chefetz B, Chen Y, Clapp CE, Hatcher PG (2000) Characterization of organic matter in soils by thermochemolysis using tetramethylammonium hydroxide (TMAH). Soil Sci Soc Am J 64:583–589
- Davis MB, Shaw RG (2001) Range shifts and adaptive responses to quaternary climate change. Science 292(5517):673–679
- DeLuca TH, MacKenzie MD, Gundale MJ, Holben WE (2006) Wildfire-produced charcoal directly influences nitrogen cycling in ponderosa pine forests. Soil Sci Soc Am J 70(2):448–453
- Di Blasi C (2008) Modeling chemical and physical processes of wood and biomass pyrolysis. Prog Energy Combust Sci 34:47–90



- FAO (2010) Global forest resources assessement. In: FAO,
- Fernández JM, Cm Peltre, Craine JM, Plante AF (2012) Improved characterization of soil organic matter by thermal analysis using CO<sub>2</sub>/H<sub>2</sub>O evolved gas analysis. Environ Sci Technol 46:8921–8927
- Filley TR, Minard RD, Hatcher PG (1999) Tetramethylammonium hydroxide (TMAH) thermochemolysis: proposed mechanisms based upon the application of <sup>13</sup>C-labeled TMAH to a synthetic model lignin dimer. Org Geochem 30(7):607–621
- Filley TR, Nierop KGJ, Wang Y (2006) The contribution of polyhydroxyl aromatic compounds to tetramethylammonium hydroxide lignin-based proxies. Org Geochem 37:711–727
- Fung BM, Khitrin AK, Ermolaev K (2000) An improved broadband decoupling sequence for liquid crystals and solids. J Magn Reson 142:97–101
- Gärdenas AI, Agren GI, Bird JA, Clarholm M, Hallin S, Ineson P, Katterer T, Knicker H, Nilsson SI, Nasholm T, Ogle S, Paustian K, Persson T, Stendahl J (2011) Knowledge gaps in soil carbon and nitrogen interactions—From molecular to global scale. Soil Biol Biochem 43(4):702–717
- Giudicianni P, Cardone G, Ragucci R (2013) Cellulose, hemicellulose and lignin slow steam pyrolysis: thermal decomposition of biomass components mixtures. J Anal Appl Pyrol 100:213–222
- Gray J, Thompson P (1977) Climatic information from <sup>18</sup>O/<sup>16</sup>O analysis of cellulose, lignin and whole wood from tree rings. Nature 270:708–709
- Hammes K, Smernik RJ, Skjemstad JO, Herzog A, Vogt UF, Schmidt MWI (2006) Synthesis and characterisation of laboratory-charred grass straw (Oryza sativa) and chestnut wood (Castanea sativa) as reference materials for black carbon quantification. Org Geochem 37:1629–1633
- Hammes K, Schmidt MWI, Smernik RJ, Currie LA, Ball WP, Nguyen TH, Louchouarn P, Houel S, Gustafsson O, Elmquist M, Cornelissen G, Skjemstad JO, Masiello CA, Song J, Peng P, Mitra S, Dunn JC, Hatcher PG, Hockaday WC, Smith DM, Hartkopf-Froder C, Bohmer A, Luer B, Huebert BJ, Amelung W, Brodowski S, Huang L, Zhang W, Gschwend PM, Flores-Cervantes DX, Largeau C, Rouzaud JN, Rumpel C, Guggenberger G, Kaiser K, Rodionov A, Gonzalez-Vila FJ, Gonzalez-Perez JA, de la Rosa JM, Manning DAC, Lopez-Capel E, Ding L (2007) Comparison of quantification methods to measure fire-derived (black/elemental) carbon in soils and sediments using reference materials from soil, water, sediment and the atmosphere. Global Biogeochem Cycles 21(GB3016):1–18
- Hammes K, Torn MS, Lapenas AG, Schmidt MWI (2010) Centennial black carbon turnover observed in a Russian steppe soil. Biogeosciences 5:1339–1350
- Harvey OR, Kuo L-J, Zimmermann AR, Louchouarn P, Amonette JE, Herbert BE (2012) An index-based approach to assessing recalcitrance and soil carbon sequestration potential of engineered black carbons (biochars). Environ Sci Technol 46:1415–1421
- IPCC (2014) Climate change 2014: impacts, adaptation, and vulnerability. In: Field CB, Barros VR, Dokken DJ, Mach KJ, Mastrandrea MD, Bilir TE, Chatterjee M, Ebi KL, Estrada YO, Genova RC, Girma B, Kissel ES, Levy AN,

- MacCracken S, Mastrandrea PR, White LL (eds) Cambridge University Press, Cambridge, pp 1132
- Jaffé R, Ding Y, Niggemann J, Vähätalo AV, Stubbins A, Spencer RGM, Campbell J, Dittmar T (2013) Global charcoal mobilization from soils via dissolution and riverine transport to the oceans. Science 340:345–347
- Keiluweit M, Nico PS, Johnson MG, Kleber M (2010) Dynamic molecular structure of plant biomass-derived black carbon (biochar). Environ Sci Technol 44(4):1247–1253
- Knicker H (2007) How does fire affect the nature and stability of soil organic nitrogen and carbon? A review. Biogeochemistry 85:91–118
- Knicker H (2011a) Pyrogenic organic matter in soil: its origin and occurrence, its chemistry and survival in soil environments. Quatern Int 243:251–263
- Knicker H (2011b) Soil organic N—An under-rated player for C sequestration in soils? Soil Biol Biochem 43(6):1118–1129
- Knicker H, Hilscher A, Gonzalez-Vila FJ, Almendros G (2008) A new conceptual model for the structural properties of char produced during vegetation fires. Org Geochem 39:935–939
- Kuo L-J, Herbert BE, Louchouarn P (2008) Can levoglucosan be used to characterize and quantify char/charcoal black carbon in environmental media? Org Geochem 39:1466–1478
- Leavitt SW, Danzer SR (1993) Method for batch processing small wood samples to holocellulose for stable-carbon isotope analysis. Anal Chem 65(1):87–89
- Lehmann J (2007) Bio-energy in the black. Front Ecol Environ 5(7):381–387
- Masiello CA (2004) New directions in black carbon organic geochemistry. Mar Chem 92:201–213
- Masiello CA, Louchouarn P (2013) Fire in the ocean. Science 340:287–288
- Masiello CA, Chen Y, Gao X, Liu S, Cheng H-Y, Bennett MR, Rudgers JA, Wagner DS, Zygourakis K, Silberg JJ (2013) Biochar and microbial signaling: production conditions determine effects on microbial communication. Environ Sci Technol 47:11496–11503
- McBeath AV, Smernik RJ (2009) Variation in the degree of aromatic condensation of chars. Org Geochem 40:1161–1168
- McBeath AV, Smernik RJ, Krull ES, Lehmann J (2014) The influence of feedstock and production temperature on biochar carbon chemistry: a solid-state <sup>13</sup>C NMR study. Biomass Bioenergy 60:121–129
- Metz G, Wu XL, Smith SO (1994) Ramped-Amplitude Cross Polarization in Magic-Angle-Spinning NMR. J Magn Reson 110:219–227
- Newton PF (2012) Simulating site-specific effects of a changing climate on jack pine productivity using a modified variant of the croplanner model. Open J For 2:23–32
- Preston CM, Schmidt MWI (2006) Black (pyrogenic) carbon: a synthesis of current knowledge and uncertainties with special consideration of boreal regions. Biogeosciences 3:397–420
- Randerson JT, Chen Y, van der Werf GR, Rogers BM, Morton DC (2012) Global burned area and biomass burning emissions from small fires. J Geophys Res Biogeosci 117:G04012
- Reich PB, Sendall KM, Rice K, Rich RL, Stefancki A, Hobbie SE, Montgomery RA (2015) Geographic range predicts



- photosynthetic and growth response to warming in co-occurring tree species. Nat Clim Change 5:148–152
- Ryan KC (2002) Dynamic interactions between forest structure and fire behavior in boreal ecosystems. Silv Finn 36(1):13–39
- Ryan MG, Melillo MM, Ricca A (1990) A comparison of methods for determining proximate carbon fractions of forest litter. Canadian J For Res Revue Can Rech For 20:166–171
- Santin C, Doerr SH, Kane ES, Masiello CA, Ohlson M, de la Rosa JM, Preston CM, Dittmar T (2015a) Towards a global assessment of pyrogenic carbon from vegetation. Glob Change Biol 22:76–91
- Santin C, Doerr SH, Preston CM, Gonzalez-Rodriguez G (2015b) Pyrogenic organic matter produced during wildfires can act as a carbon sink. Glob Change Biol 21(4):1621–1633
- Santos F, Torn MS, Bird JA (2012) Biological degradation of pyrogenic organic matter in temperate forest soils. Soil Biol Biochem 51:115–124
- Scheirs J, Camino G, Tumiatti W (2001) Overview of water evolution during the thermal degradation of cellulose. Eur Polymer J 37:933–942
- Schmidt MWI, Torn MS, Abiven S, Dittmar T, Guggenberger G, Janssens IA, Kleber M, Koegel-Knabner I, Lehmann J, Manning DAC, Nannipieri P, Rasse DP, Weiner S, Trumbore SE (2011) Persistence of soil organic matter as an ecosystem property. Nature 478(7367):49–56
- Schneider MPW, Hilf M, Vogt UF, Schmidt MWI (2010) The benzene polycarboxylic acid (BPCA) pattern of wood pyrolyzed between 200°C and 1000°C. Org Geochem 41:1082–1088
- Serra O, Chatterjee S, Figueras M, Molinas M, Stark RE (2014)
  Deconstructing a plant macromolecular assembly: chemical architecture, molecular flexibility, and mechanical performance of natural and engineered potato suberins.

  Biomacromolecules 15:799–811
- Singh BP, Cowie AL, Smernik RJ (2012a) Biochar carbon stability in a clayey soil as a function of feedstock and pyrolysis temperature. Environ Sci Technol 46:11770– 11778

- Singh N, Abiven S, Torn MS, Schmidt MWI (2012b) Firederived organic carbon in soil turns over on a centennial scale. Biogeosciences 9:1–11
- Smernik RJ, Baldock JA, Oades JM (2002) Impact of remote protonation on <sup>13</sup>C CPMAS NMR quantitation of charred and uncharred wood. Solid State Nucl Magn Reson 22:71–82
- Solum MS, Pugmire RJ, Jagtoyen M, Derbyshire F (1995) Evolution of carbon structure in chemically activated wood. Carbon 33(9):1247–1254
- Soucémarianadin LN, Quideau SA, MacKenzie MD, Bernard GM, Wasylishen RE (2013) Laboratory charring conditions affect black carbon properties: a case study from Quebec black spruce forests. Org Geochem 62:46–55
- Soucémarianadin LN, Quideau SA, MacKenzie MD (2014) Pyrogenic carbon stocks and storage mechanisms in podzolic soils of fire-affected Quebec black spruce forests. Geoderma 217–218:118–128
- Sperry JS, Hacke UG, Pitterman J (2006) Size and function in conifer tracheids and angiosper vessels. Am J Bot 10:1490–1500
- Wang Z, McDonald AG, Westerhof RJM, Kersten SRA, Cuba-Torres CM, Ha S, Pecha B, Garcia-Perez M (2013) Effect of cellulose crystallinity on the formation of a liquid intermediate and on product distribution during pyrolysis. J Anal Appl Pyrol 100:56–66
- Werner K, Pommer L, Brostrom M (2014) Thermal decomposition of hemicelluloses. J Anal Appl Pyrol 110:130–137
- Wiedemeier DB, Abiven S, Hockaday WC, Keiluweit M, Kleber M, Masiello CA, McBeath AV, Nico PS, Pyle LA, Schneider MPW, Smernik RJ, Wiesenberg GLB, Schmidt MWI (2015) Aromaticity and degree of aromatic condensation of char. Org Geochem 78:135–143
- Wind RA, Li L, Maciel GE, Wooten JB (1993) Characterization of electron spin exchange interactions in cellulose chars by means of ESR, <sup>1</sup>H NMR, and dynamic nuclear polarization. Appl Magn Resonance 5(2):161–176
- Zimmermann AR (2010) Abiotic and microbial oxidation of laboratory-produced black carbon (biochar). Environ Sci Technol 44(4):1295–1301

